CHAPTER IV
PREPARATION AND CHARACTERIZATION OF POLYAMIDE11/BACTERIAL NANOCOMPOSITE FILMS

4.1 Abstract

The flexible piezoelectric films of polyamide 11 (PA11)/bacterial cellulose (BC) were prepared via solution casting and casted by compression method as a thin films. The various weight percentage of extracted BC (0.2, 0.4, 0.6, 0.8, 1wt%) were incorporated into PA11 matrix using formic acid as a solvent. The results showed that higher amount of BC can slightly increase thermal stability, crystallinity and mechanical properties of the nanocomposite, but it made the composite less transparent. The tensional behavior of nanocomposite films was improved compared with neat PA11, Young's modulus was increased from 678 to 749Mpa at 1wt% of BC. Noncentrosymmetry structure of odd-numbered polyamide and the dipole orientation under an applied field induce the polarization yielding the good dielectric and piezoelectric properties. Inclusion of BC additionally increase dielectric and piezoelectric properties due to the interfacial polarization that might be generated at the interfaces between fiber and polymer matrix.

4.2 Introduction

Touchscreen has been one of the most popular technologies for electronic devices. Several applications such as smart phone, tablet, smart watch are required this technology. Piezoelectric touch sensor, the unpopular touch technology was introduced to overcome the limitations of common touch technology by combined the benefits of both capacitive and resistive touch sensors. The piezo/ferroelectric polymer materials have been discovered and are currently being investigated, including cyanopolymers, polyuria, polythioureas, aromatic polyamides, odd-numbered polyamide, and biopolymers (Lewis et al., 1997). Odd-numbered polyamide, such as polyamide 7 and polyamide 11, are of interest due to their polar crystal structure and thermal stability from the point of view of piezoelectricity.

(Sampson *et al.*, 2012). Nowadays, polyamide or nylon has been widely used as one of the most important thermoplastics because of its good thermal stability, fire resistance and mechanical properties (Bak *et al.*, 2010; Ding *et al.*, 2009). Piezoelectric and ferroelectric properties of odd-numbered polyamide have been studied and showed that the piezoelectric responses of odd-numbered polyamide is temperature dependent and larger than that in PVDF at higher temperatures above their glass transition temperature, Tg. The piezoelectric constant increase rapidly with temperature maximum stable d31 value of 17 pC/N and 14 pC/N are reported for polyamide 7 and polyamide 11. howover, the thermal expansion coefficient, CTE of polyamide is about 110 ppm/k. This films of polyamide will be limited by this effect due to shrinkage at high temperature. To solve this problem, the bacterial cellulose that has low CTE will be added. Bacterial cellulose is nano-size cellulose product of bacteria Acetobacter xylinum, that has very low CTE which is 0.1 ppm/K (Nogi *et al.*, 2008). The proposed work aims to fabricate the thin film nanocomposite derived by the polar odd-numbered polyamide and the bacterial cellulose fiber. The ultimate piezoelectric properties coupling with good thermal and mechanical properties are required. The optimized ratio between BC and polyamide will be investigated including the measurement of all related properties.

4.3 Experimental Procedures

4.3.1 Materials

Nata de coco was purchased from local food market. PA11 was purchased from Sigma-Aldrich Co., Ltd. Formic acid (AR grade, 99%) and sodium hydroxide (NaOH) (AR grade, 98%) were purchased from S.M. Chemical Co., Ltd. and Labscan Ltd., respectively.

4.3.2 BC preparation (Pakdeepatarapun *et al.*, 2014)

Nata de coco gel was firstly washed with water to remove some excess sugar. After that the washed nata de coco gel was grinded and treated with 0.1 M NaOH at 80 °C for 2 h to obtain the BC pellicles. The BC pellicles were then

washed with hot deionized water until neutral pH is reached. The BC pellicles were dispersed in deionized water and kept in bottle.

4.3.3 Fabrication of PA11/BC Nanocomposite Films

BC paste was rinsed with formic acid to remove all water content. Then BC dispersed in formic acid was obtained. Polyamide dissolved in formic acid is mixed with BC dispersed in polyamide with the percentage weight at 0.2 , 0.4, 0.6, 0.8, 1. Then the mixture solution was mixed by mechanical stirrer at 80°C for 10 minutes or until PA11 fully dissolved in formic acid and taken into the ultrasonic bath to obtain better dispersion for an hour. The mixture solution will be further dropped into clean cool water for 10 minutes. After that they are heated in oven at 70 °C for 2 days. The blend will be obtained., the casted blend films were obtained. Finally, the casted film were performed by a compression press (Wabush, model No.V50H-15-RPX, 4-post design) with preheating for 5 min, followed by compressing for 5 min at 5 Tons. The operating temperature of mold was maintained at 220 °C.

4.3.4 Characterizations

The morphology of BC samples were observed through transmittance electron microscope (TEM, JEOL-2100). The thermal properties were investigated by differential scanning calorimeter (DSC, METTLER, DSC822) and thermal gravimetric analyzer (TGA, Perkin Elmer). X-rays diffraction microscope (XRD, Rigaku, SmartLab) were used to determine crystalline phases of the nanocomposite films. Tensile properties were investigated follow the ASTM D882. The optical property was determined by using UV/Vis spectrophotometer (Shimadzu 2550). The dielectric constant and dissipation factor were measured using a Network Analyzer (Agilent, E4991A).

4.4 Results and Discussion

4.4.1 BC Characterization

4.4.1.1 Crystallinity of BC

The crystallinity of Bacterial Cellulose sheet prepared from nata de coco measured by X-ray diffractometer. The X-ray diffraction pattern of Bacterial cellulose was shown in Figure 4.1. The result showed three clearly diffraction peak occurring at 2θ approximately at 14.5°, 16.9° and 22.5° which refered to the 110, 110 and 200 diffraction plane respectively. The result was confirmed for crystal lattice of "cellulose I" which consisted of two crystal structure which was cellulose I_α and I_β.

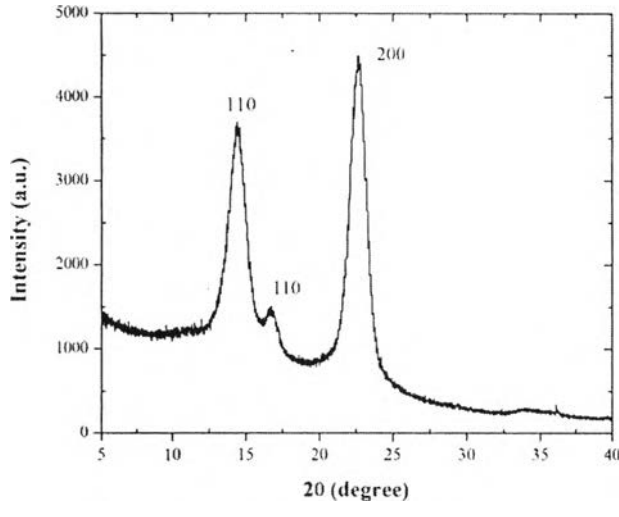

Figure 4.1 X-ray diffraction pattern of BC from nata de coco.

4.4.1.2 Chemical Functionality of BC

The FT-IR spectra of BC is shown in Figure 4.2. The structure of BC is linear homopolymer composed of D-glucopuranose units linked by β-1,4-glycosidic linkage at C_1 and C_4 carbon position (O-Rak, 2013). The peak at 3348 cm^{-1} was assigned to O-H stretching while the peak at around 2900 cm^{-1} was assigned to C-H stretching. The peak at 1163 cm^{-1} and 1033 cm^{-1} was assigned to ether bonding and methoxyl group, respectively.

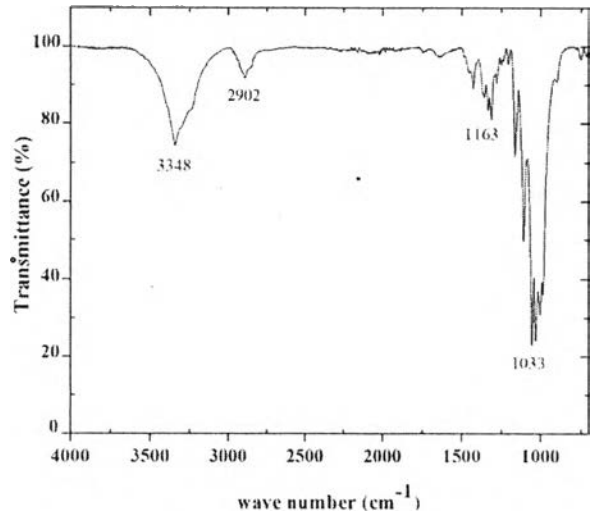

Figure 4.2 FT-IR Spectra of neat BC sheet.

4.4.1.3 Morphological Observation of BC

Figure 4.3 (a) and (b) showed TEM images of BC with different scales. This TEM images were used to determine structure and diameter of BC. The images showed that the structure of BC was networking structure with nano-scale diameter approximately 30-50 nm leaded to high optical properties of B. Due to the network structure from Figure 4.3 (a), the high surface area was obtained because of an increase in the interaction between hydroxyl groups on BC and polar groups in polymer matrix which obtained high mechanical properties (Phakdeepataraphan et al., 2014).

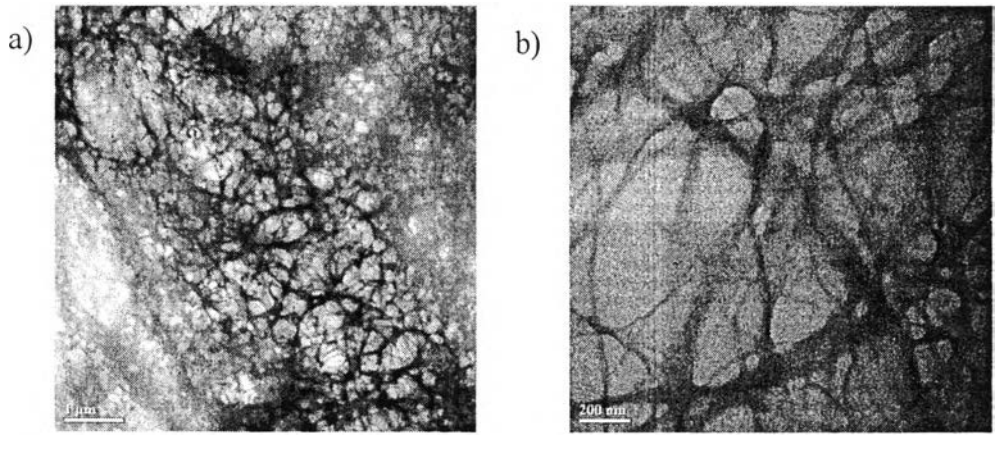

Figure 4.3 TEM images of BC at magnification of (a) 50 (b) 200.

4.4.1.4 Thermal Properties

TGA measurement was used to identify the thermal degradation and %weight loss of bacterial cellulose. The sample was measured from 30 to 900 °C under nitrogen atmosphere at rate of 20 ml/min and heating rate of 10 °C/min. Figure 4.4 showed TGA thermogram of bacterial cellulose which was plotted of remaining weight versus temperature. The result indicated that there were 2 thermal degradation steps. The first step was occurred at 100 °C which referred to the water evaporation of remaining water in bacterial cellulose. The other step was observed at 250 °C which referred to the degradation of bacterial cellulose. Finally, there was some remaining weight which was indicated to char formation occurring from degradation step.

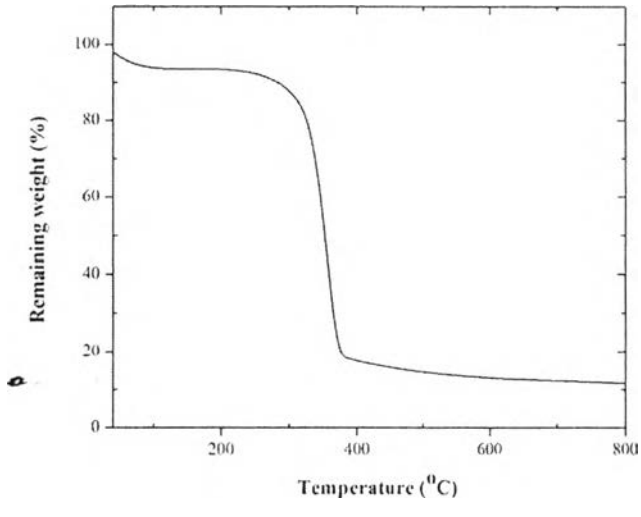

Figure 4.4 TG-DTA thermogram of BC sheet.

4.4.2 PA11/BC nanocomposite Films Characterization

4.4.2.1 Morphological Properties

Figure 4.5 shows a cross-sectional SEM images of PA11/BC compared with neat PA11 at the magnification of 1 k. With the higher amount of BC content, the toughness of the blend film tended to be decreased which can be confirmed by the sample's surface fracture. The hole in Figure 4.5 shows the hole of BC that was pulled out from PA11 matrix that indicated the interaction between

PA11 and BC is strong due to the poor adhesion between fiber surface and PA11 matrix.

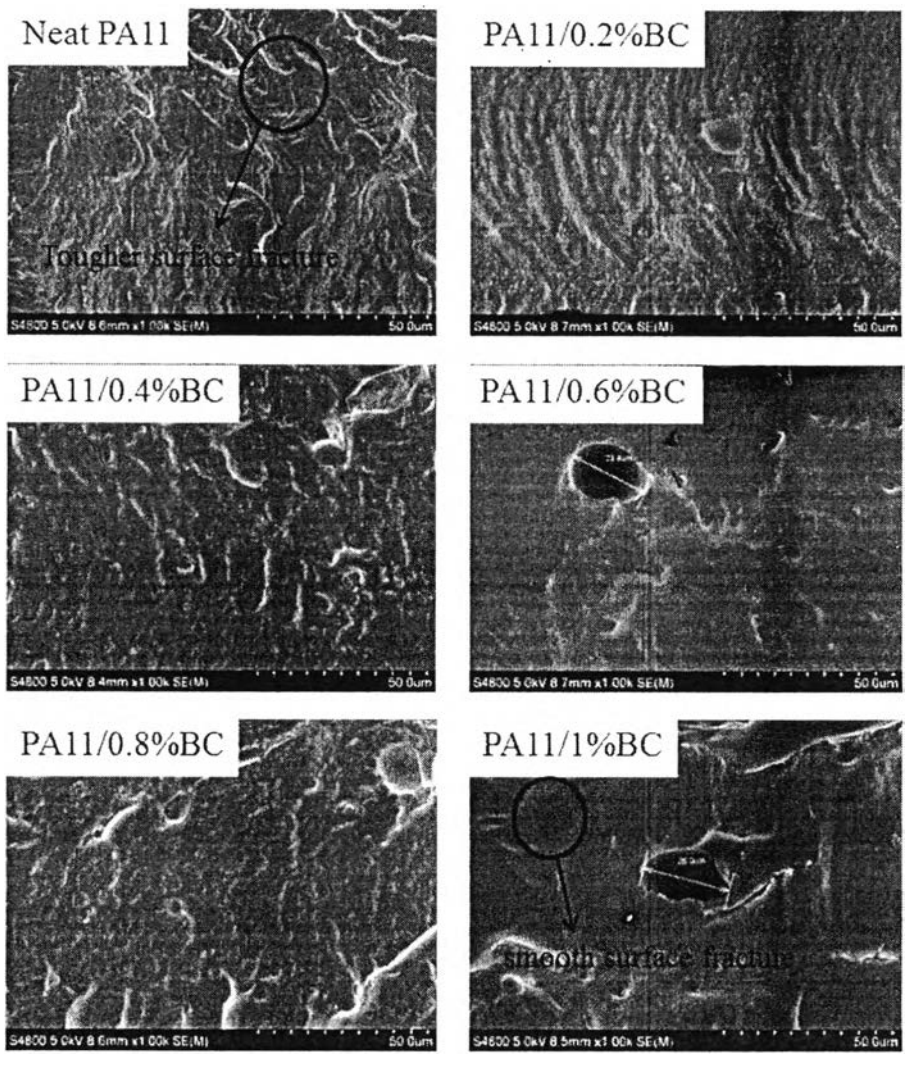

Figure 4.5 SEM images of PA11/BC blend films at different weight compositions at magnification of 1 k.

4.4.2.2 Crystalline Phase Behavior

PA 11 has been found to have at least four, possibly five, crystal forms : two triclinic forms (α and α′) and three monoclinic forms (γ, δ, δ′). The most common form is α form. The X-ray patterns for α and α′ forms are very

similar, with only small differences in the d-spacings. Likewise, the patterns for the γ, δ and δ′ forms are similar. The δ and δ′ forms are quite possibly the same crystal structure but differing degree of order. In the γ form the molecular chains are slightly contracted form that of the fully extended planar zigzag found in the α form of PA (Hsin H.Y., 1998).

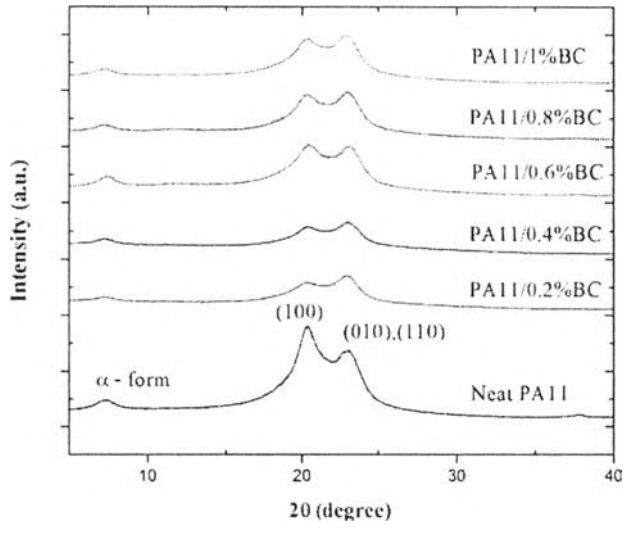

Figure 4.6 X-ray diffraction patterns of PA11/BC nanocomposite films compared with neat PA11.

Figure 4.6 shows XRD patterns of crystalline phase of PA11/BC nanocomposite films with 0.2, 0.4, 0.6, 0.8 and 1 wt% of BC loading compared with neat PA11.It can be seen two strong reflections (100) and (010,110) at the diffraction angle 2θ of 20.02° and 23.01°, which are the triclinic α-form (Zhang, Q. *et al*, 2001). From the XRD result. When the amount of BC was increased at 0.2wt%, the triclinic α-form (100) tended to decrease as can be confirmed by the decreasing of the height of diffraction peak at 20.02° and also the decreasing of 23.01° peak height, but after added BC higher than 0.2wt%, the triclinic α-form tended to increase. In addition, when the amount of BC more than 0.2 wt%, the peak at 20.02° and 23.01° will be increase.

4.4.2.3 Thermal Properties

Thermal degradation behavior of Polyamide11/Bacterial Cellulose nanocomposite film was measured by using TGA as shown in Figure 4.7. The result showed that the degradation started at 350°C which referred to degradation temperature of PA11 and the result demonstrated that bacterial cellulose had no effect to improve the thermal stability of PA11 polymeric chain. The nanocomposite films were free from formic acid due to the absence of thermal degradation at 100.8 °C, which was the boiling point of formic acid.

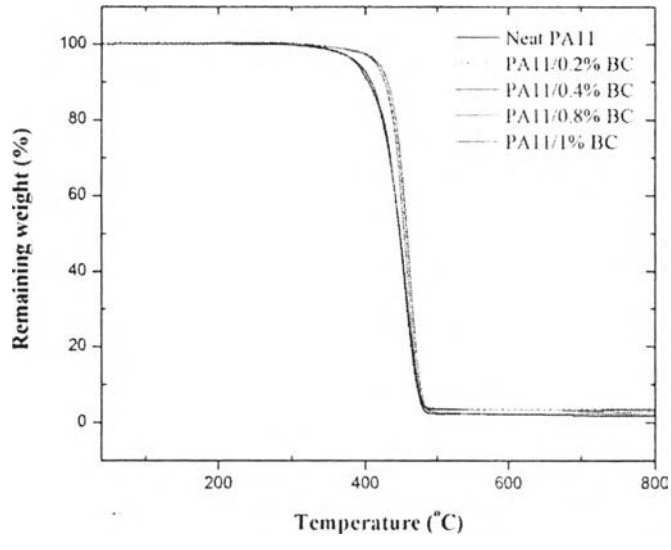

Figure 4.7 TG-DTA thermograms of PA11 nanocomposite films.

The DSC parameters are shown in Table 4.1. From the result, there was one transition temperature observed at 188 °C and 165 °C which corresponding to T_m and T_c of PA11. Figure 4.9 shows the second-heating curves of PA11/BC nanocomposite films. BC has effects on PA11 crystallinity (X_C) but has no effect on T_m. The results show that increasing of BC content up to 0.2 wt% can slightly decrease X_C, this occurred due to the BC may be disturbed PA crystallization. However, he amount of BC more than 0.2 wt%, X_c tended to increase, this may occur due to orientation and dispersion of BC resulted to higher possibility of PA11

chains to come close and crystallize. The crystallinity temperature are showed in Figure 4.9, indicate that higher amount of BC has no effect to PA11 crystallinity.

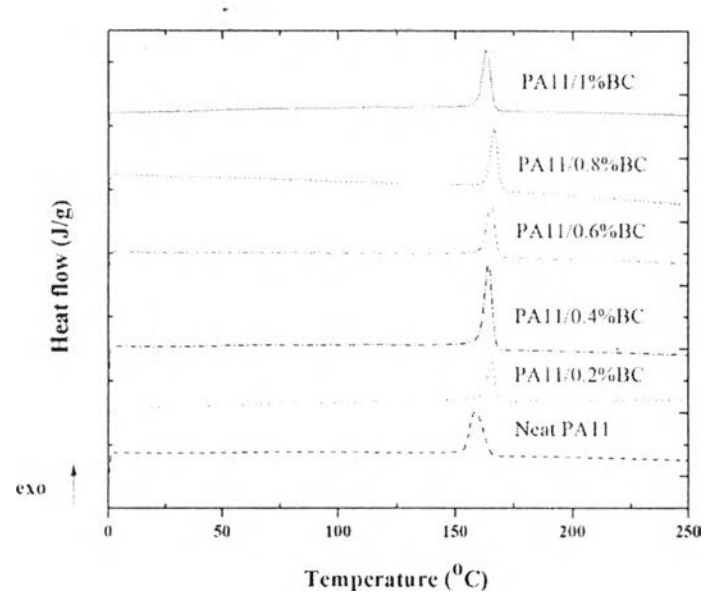

Figure 4.8 DSC second-heating curves of PA11/BC nanocomposite films.

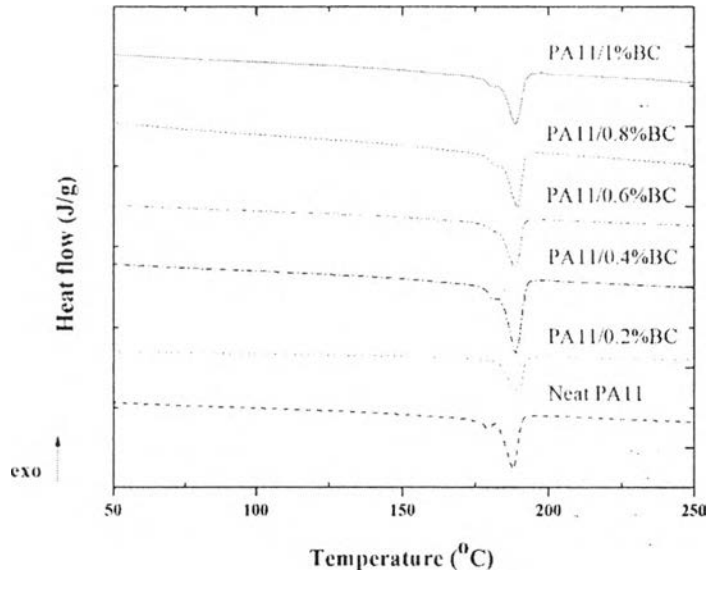

Figure 4.9 DSC first-cooling curves of PA11/BC nanocomposite films.

Table 4.1 DSC parameters of PA11/BC mamocomposite films compared with neat PA11

Sample	ΔH_m (J/g)	T_m (°C)	X_c (%)	T_c (°C)
Neat PA11	51.85	187.5	25.17	159
PA11/0.2%BC	41.53	188.5	20.16	165.9
PA11/0.4%BC	59.73	188.2	29	165
PA11/0.6%BC	57.15	188.2	27.74	165.6
PA11/0.8%BC	60.07	188.9	29.16	167.3
PA11/1%BC	61.08	188.3	29.65	164.1

*Heat of fusion value for 100% crystalline PA11, ΔH_m^o = 206 J/g

4.4.2.4 Mechanical Properties

With the incorporation of BC, the nanocomposite films become more brittle as can be seen in Figure 4.12 which corresponded to SEM images in figure 4.5 that showed the tough surface fracture. Figure 4.10, BC provided slightly higher Young's modulus to the blend films compared with neat PA11 but BC provided decreased on the tensile strength of the nanocomposite as can be seen in Figure 4.11 which corresponded to SEM images that show no interaction between polymer matrix and filler and poor distribution of BC in films that make the tensile strength decreased.

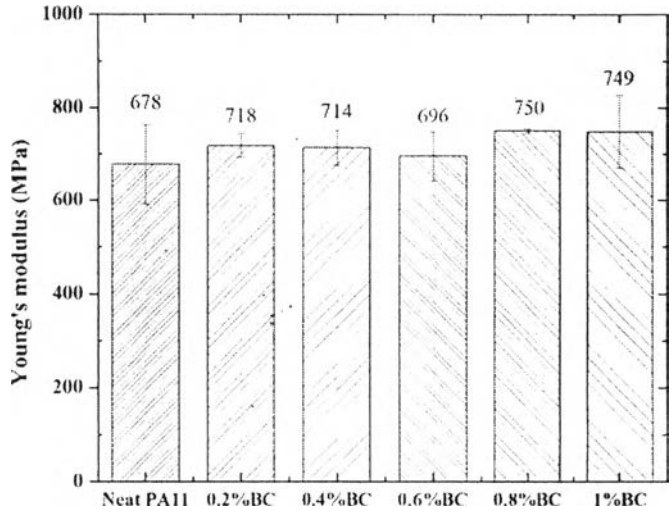

Figure 4.10 Young's modulus of PA11/BC nanocomposite films.

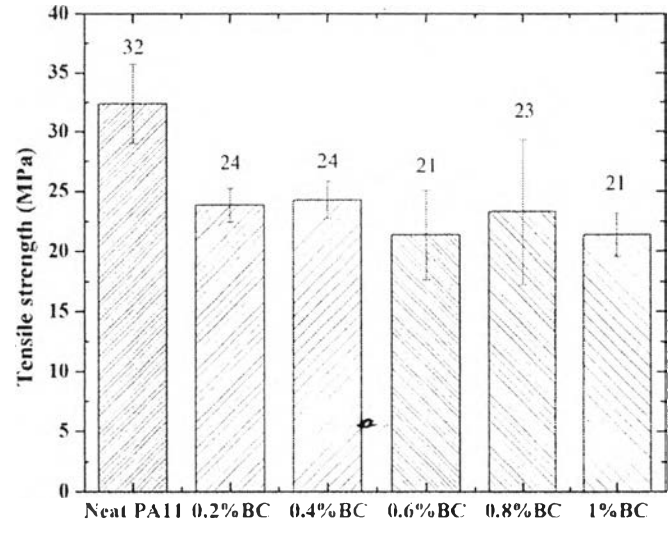

Figure 4.11 Tensile strength of PA11/BC nanocomposite films.

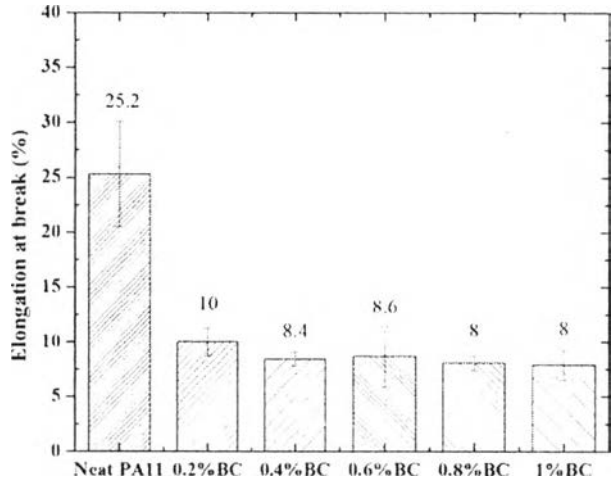

Figure 4.12 Elongation at break of PA11/BC nanocomposite films.

4.4.2.5 Dynamic Mechanical Properties

The dynamic mechanical properties as a function of temperature as various amount of BC in PA11/BC nanocomposite films compared with neat PA11 are shown in Figure 4.13. As the amount of BC increase, the storage modulus also slightly increases throughout the temperature range from 0 °C to 150 °C.

There is relaxation region, in the Figure 4.14, this relaxation was referred to α relaxation state. α-relaxation shows the dynamic glass transition temperature (T_g) of material which was found at 40°C. The incorporation of BC in the blend films that cause higher glass transition temperature to PA11 because the BC interrupt the chain of PA11 that cause the chain harder to move. Consequently, the glass transition temperature shifted forward to higher temperature from 40°C to 60°C with increasing BC content.

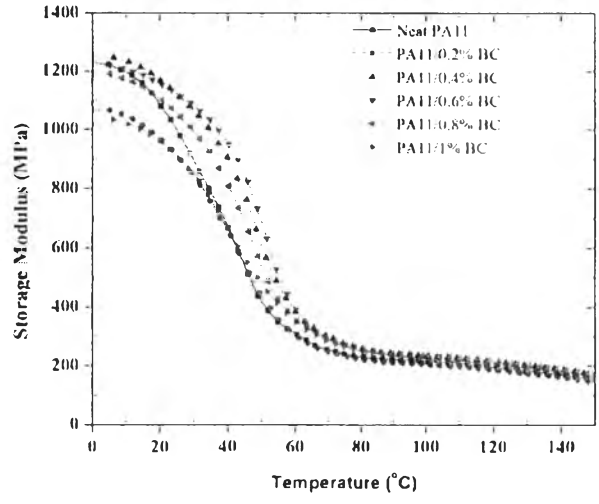

Figure 4.13 Storage tensile modulus, E' vs temperature of various amounts of BC in PA11/BC nanocomposite films compared to neat PA11.

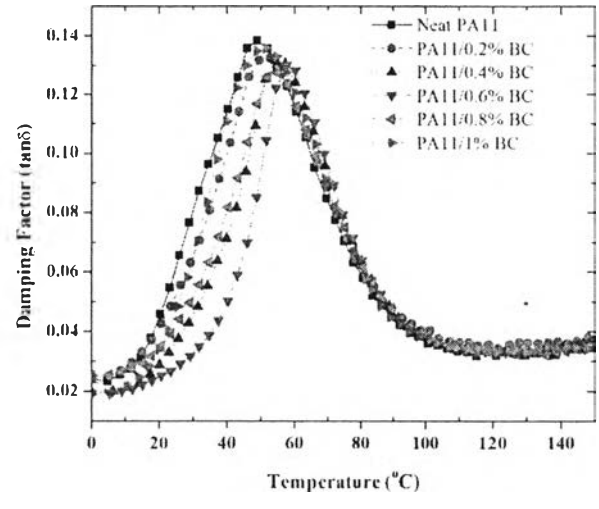

Figure 4.14 Damping factor (E"/E') vs temperature of various amounts of BC in PA11 nanocomposite films compared to neat PA11.

4.4.2.6 Optical Properties of PA11/BC nanocomposite Films

Figure 4.15 shows the appearances of nanocomposite films. it was found that the films appearances become more opaque with the increasing of BC weight percentage, this optical result can be confirmed by Figure 4.16 which shows UV/Vis spectra of the neat PA11 and PA11/BC nanocomposite films and reference is

neat PA11. Neat PA11 has 60-100% transmittance in the visible light region (400-800 nm), but when adding BC, the transmittance tends to decrease, which means BC exhibits the opacity property. It is due to the crystallization of nanocomposite films because PA can form crystal quickly after compression process and from crystalline results, crystalline of BC and PA11 that made the transmittance tends to decrease.

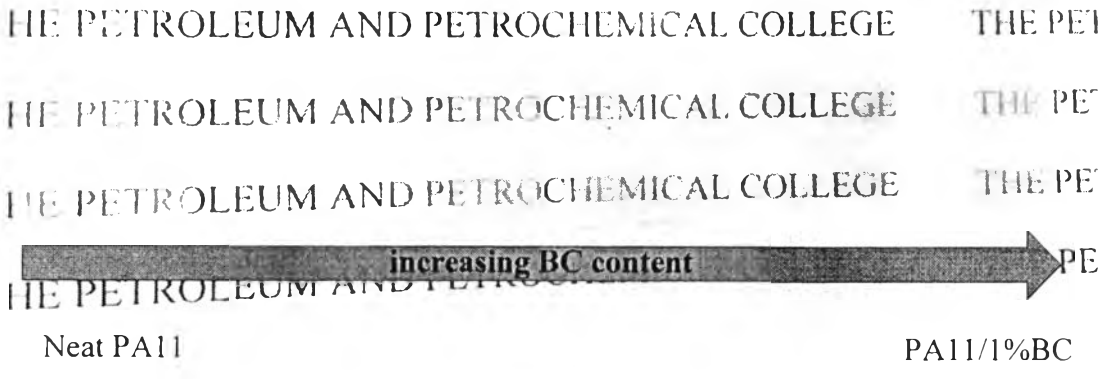

Figure 4.15 Sample appearances of PA11/BC nanocomposite films compared with neat PA11.

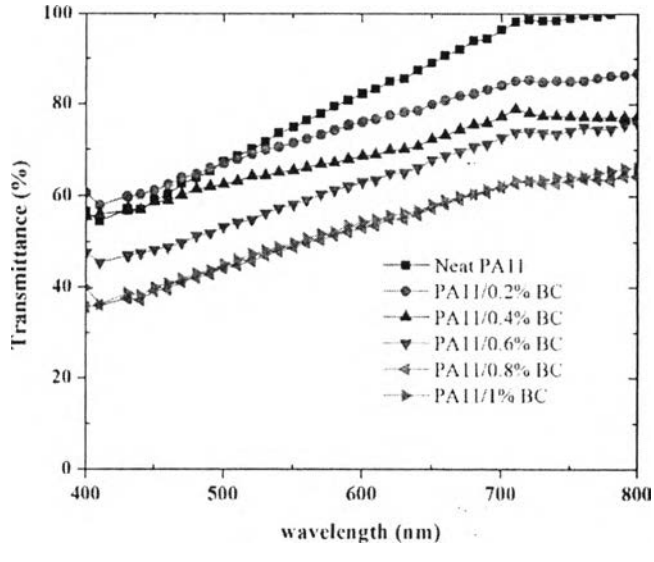

Figure 4.16 UV/Vis spectra of PA11/BC blend films compared with neat PA11.

4.4.2.7 Dielectric Properties of PA11/BC nanocomposite Films

The dielectric constant related to piezoelectric properties via the equation "$d_{ij} = \varepsilon_{ii} g_{ij}$" , where d_{ij} is stress piezoelectric coefficient, ε_{ii} is the permittivity of the material and g_{ij} is strain piezoelectric coefficient and ε_o is the vacuum dielectric constant permittivity (8.85×10^{-12} F/m). This equation shows that the dielectric property is a basis property for piezoelectric materials. In this part, the effect of frequency, temperature and BC content on dielectric behavior of PA11/BC nanocomposite films and neat PA11 were discussed.

Figure 4.17 shows dielectric constant (a) and dissipation factor (b) of neat PA11 and PA11/BC nanocomposite films at 0.2, 0.4, 0.6, 0.8 and 1 wt% of BC loading as a function of frequency (10 MHz - 1 GHz) at room temperature. Compared to neat PA11, adding with 1 wt% BC exhibited higher dielectric constant because BC can induced the interfacial polization of PA causing higher dielectric constant. For dissipation factor on frequency dependent, dissipation factor slightly decreases with increasing frequency.

The dielectric properties on temperature dependence was at wide range of frequency at 10MHz, 100MHz and 1GHz of the PA11/BC nanocomposite films compare with neat PA11 were shown in Figure 4.18. At constant frequency with high temperature, the dielectric constant tended to be high due to PA11 chains can vibrate, move and reorient which allowing them to keep up with the changing electric field which causing the dielectric constant increased. With lower temperature, the segmental motion of the chain is practically frozen when the temperature was much lower than dynamic T_g which causing the lower dielectric constant. Figure 4.18 (a) shows dielectric constant at 10MHz the dipoles in polymeric chain had sufficient time to align with the electrical field direction causing to the higher dielectric constant. With higher frequency, the dipoles had short time to align with the electrical field direction causing the lower dielectric constant. It can be concluded that the dielectric behaviors of PA11/BC and neat PA11 strongly depend on the variation of frequency and temperature.

Figure 4.19 shows the dielectric constant before poling by corona discharge at 120°C, 8KV/mm for 20 minutes, Figure 4.19 (a) the dielectric constant of PA/BC is around 2-2.5 at various weight percent of BC at 0.2-1 wt%.

After poling, the dielectric constant was increased from 2-2.5 to 2.3- 3.3 as shown in Figure 4.19 (b) because the electric field can align the polar of PA11 in the same direction and also the noncentrosymmetry structure of odd-numbered PA that cause the dielectric constant tend to increase. The electric field has no effect on dissipation factor (tanδ) as shown in Figure 4.20.

This increasing occurred due to the interfacial polarization between the hydroxyl group in the BC chain and amide group in PA chain, higher amount of polar hydroxyl group in BC, and the higher dielectric constant of nanocomposite films.

a)

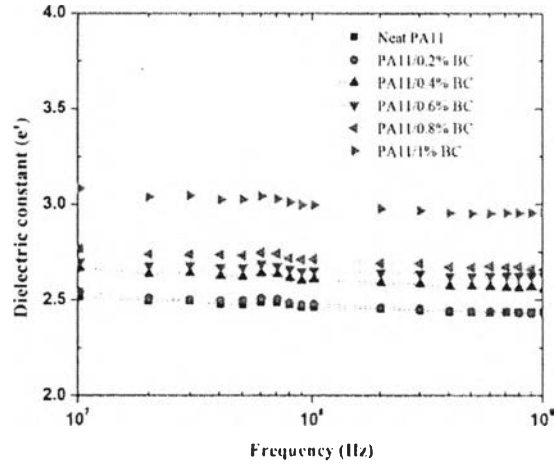

b)

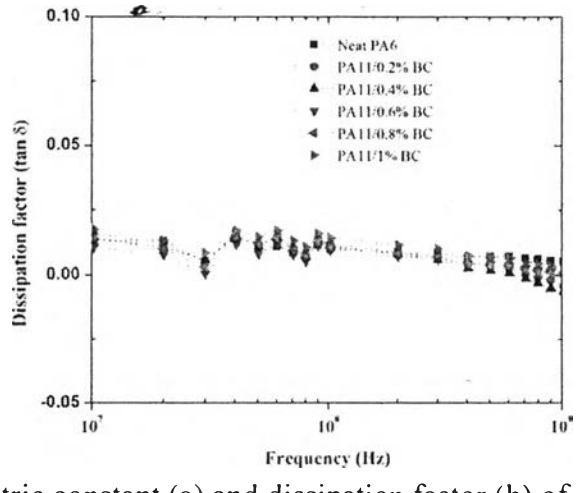

Figure 4.17 Dielectric constant (a) and dissipation factor (b) of PA11 and PA11/BC nanocomposite films as a function of frequency at 20°C.

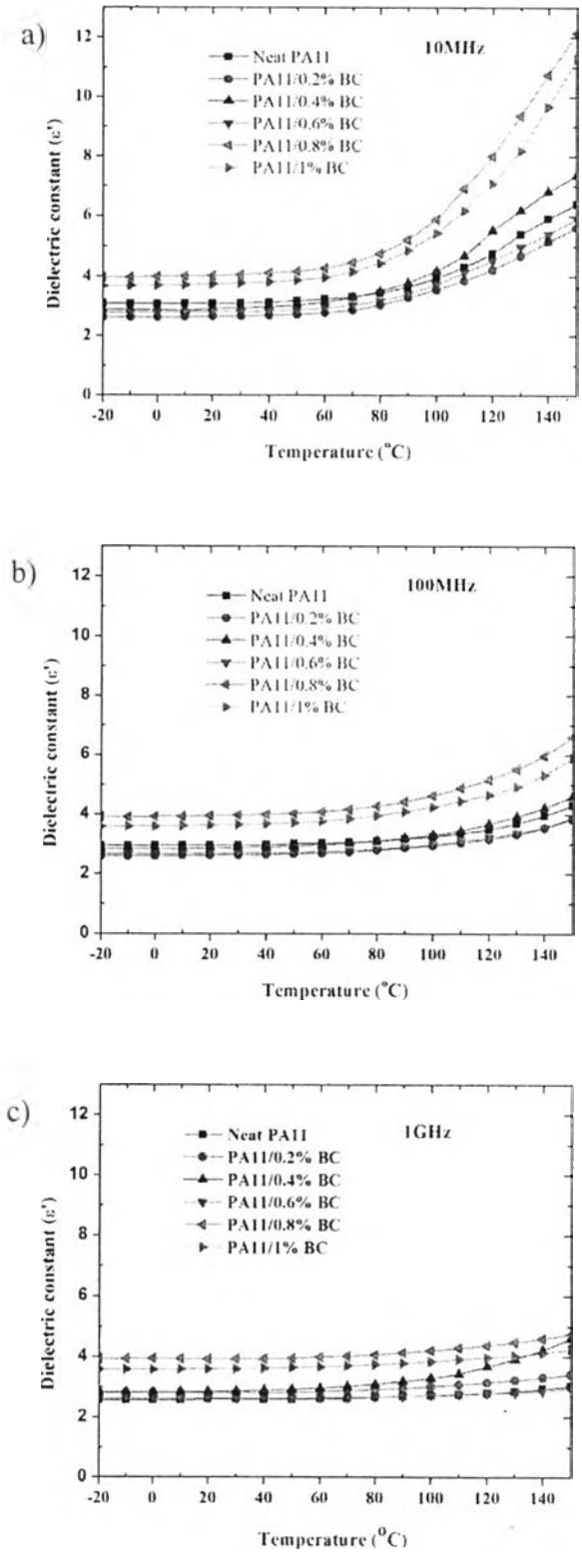

Figure 4.18 Dielectric constant of PA11/BC nanocomposite films compared with neat PA11 at temperature -20 °C – 150 °C and (a)10 MHz, (b) 100 MHz and(c) 1 GHz.

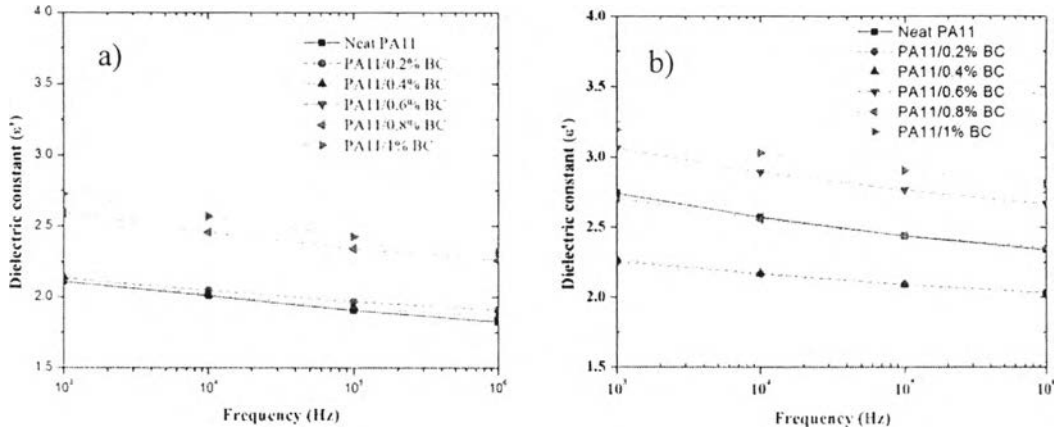

Figure 4.19 Dielectric constant (a) before poling (b) after poling of PA11 and PA11/BC nanocomposite films as a function of frequency at 20°C.

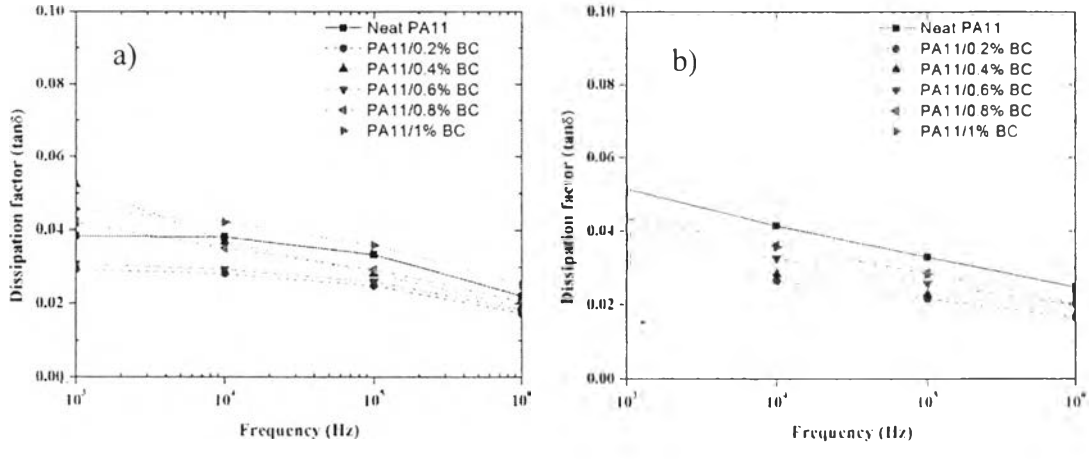

Figure 4.20 Dissipation factor (a) before poling (b) after poling of PA11 and PA11/BC nanocomposite films as a function of frequency at 20°C.

4.5 Conclusion

Polyamide 11 (PA11) was mixed with bacterial cellulose (BC) by using solution casting method using formic acid as solvent. Then casted nanocomposite films were prepared by hot-compressed method. The TEM images indicated that BC has nano-scale diameter around 30-50 nm formimg a network structure which yield

to high surface area and create more intermolecular interaction between hydrogen atoms and amide bonds. These nanocomposite films show the phase of triclinic α-phase crystallinity that was increased as increasing BC content. Young's modulus of nanocomposite films were higher than neat PA11 as increasing BC content. BC has effects on PA11 crystallinity (X_C) but has no effect on T_m and T_d. The storage modulus of the nanocomposite films was higher than neat PA11. The partially interactions between the interface of BC and PA11 yield to enhance of dielectric properties and the poling process can cause the dielectric constant tend to increase. However, for the optical property, the incorporated of BC decreased the percentage of transmittance in all visible light range.

4.6 Acknowledgement

This work has partially been supported by the Petroleum and Petrochemical College, Chulalongkorn University.

References

Bak, H., Cho, S.Y., Yun, Y.S., Jin, H.J., (2010). Electrically conductive transparent films base on nylon 6 membranes and single-walled carbon nanotube. Current Applied Physics, 10, 468-472.

Balasubramanian, V., Kelkar, D.S., Kurup, M.B., (1996). Electric conduction in ion implanted nylon-6 films. Nuclear Instruments and Methods in Physics Research B, 113, 257-260

Bhavna, V.M., Patil, S.V. (2014). Physical, structure, mechanical and thermal characterization of bacterial cellulose by G. hansenii NCIM 2529. Carbohydrate Polymers, 106, 132-141.

Czaja, W., Krystunowicz, A., Bielecki, S., Brown Jr., R.M. (2006). Microbial cellulose-the natural power to heal wounds. Biomaterials, 27, 145-151.

Fukada, E. (2000). History and recent profress in piezoelectric polymers. IEEE Transactions on Ultrasonics, Ferroelectrics, and Frequency Control, 47(6), 1277-1290.

Gang, W., Yano, O., Soen, T. (1985). Dielectric and piezoelectric properties of nylon 9 and nylon 11. Polymer Journal, 18(1), 51-61.

Harrison, J.S. and Z. Ounaies (2001). Piezoelectric Polymers. ICASE. Virginia: National Aeronautics and space Administration.

Miri, V., Persyn, O., Lefebvre, J.M., Seguela, R. (2009). Effects of water absorption on the plastic deformation behavior of nylon 6. European Polymer Journal, 45, 757-762.

Nasrullah, S., Ul-Islam, M., Khattak, W.A., Park, J.K. (2013). Overview of bacterial cellulose composites: A multipurpose advanced material. Carbohydrate Polymers, 98, 1585-1598

Nogi, M., Yano, H. (2008). Transparent nanocomposites based on cellulose produced by bacterial offer potential innovation in the electronic device. Advanced Materials, 20(10), 1848-1852

Page, I.B. (2000). Polyamide as engineering thermoplastic materials. Rapra Review Reports. Poland: Rapra Technology LTD.

Peter, F., Kreammer, A., Neumann, W., Gerhard-Multhaupt, R. (2004). Dielectric relaxation in piezo-, pyro- and ferro electric polyamide 11. IEEE Transactions in Dielectrics and Electrical Insulation, 11(2), 271-279.

Peter, F.V., Cardona. T.D., Nout, M.J.R., Gooijer, K.D.D., Heuvel, J.C.V.D. (2000). Location and limitation of cellulose production by acetobactor xylinum established from oxygen profiles. Journal of Bioscience and Bioengineering, 89(5), 414-419.

Ramona-Daniela, P., Stoica-Guzun, A., Stroescu, M. (2014). Composite films of poly(vinyl alcohol)-chitisan-bacterial cellulose for drug controlled release. International Journal of Biological Macromolecules, 68, 117-1240.

Sampson, K.A., Mishra, A.K., Waghmare, U.V. (2012). Dielectric and piezoelectric responses of nylon-7: A first-principles study. Journal of Polymer, 53(2751-2757).

Takase, Y., Lee, J.W., Scheinbeim, J.I., Newman, B.A. (1991). High-temperature characteristic of nylon-11 and nylon-7 piezoelectrics. Macromolecules, 24, 6644-6652.

Thi, T.N., Sugiyama, J., Bulone, V. (2010). Bacterial cellulose-based biomimetic composite. Biopolymer. Hirishima: Biomass Technology Research Centre, National Institute of Advanced Industrial Science and Technology.

Tulsyan, K. (2007). Amorphous polyamide nanocomposite: Effects of Stability of The Nanoclay Modifier. Massachusetts: Department of Plastic Engineering, University of Massachusetts Lowell.

Ul-Islam, M., Khan, T., Park, J.K. (2012). Nanoreinforced bacterial cellulose-montmorillonite composites for biomedical applications. Carbohydrate Polymer, 89, 1189-1197.

Ul-Islam, M., Khan, T., Park, J.K. (2012). Water holding and release properties of bacterial cellulose obtained by in situ and ex situ modification. Carbohydrate Polymers, 88, 596-603.

Vijaya, M.S. (2013). Applications in engineering and medical sciences, Piezoelectric Materials and Devices. New York: Taylor and Francis Group.

Yanhuai, D., Zhang, P., Jiang, Y., Xu, F., Yin, J., Zuo, Y., (2009). Mechanical properties of nylon-6/SiO_2 nanofiber prepared by electrospining. Materials Letters, 63, 34-36.

Zhang, Q., Mo, Z., Zhang, H., Liu, S., Cheng,S., (2001). Crystal transitions of nylon11 under drawing and annealing. Polymer, 42, 5543-5547.